TRANSPORT IN ROBUST FULLERENE-TUBE HETEROSTRUCTURE TRANSISTOR

Per Hyldgaard*[1] and Bengt I. Lundqvist*

*Dept. of Applied Physics, Chalmers University of Technology and Göteborg University,
S-41296 Gothenburg, Sweden

Abstract

A fullerene-tube (nanotube) heterostructure produces a robust resonant-tunneling transistor when leads of metallic nanotubes surrounds a short barrier of semiconducting nanotube and when a close metallic gate regulates the energy position of the resonant level trapped in this barrier region. We combine electron-structure calculations with a conserving nonequilibrium Green function study for the interacting transistor transport to describe the predicted current-switch, transistor, and negative-differential amplification effects. The potential for electron dynamics inside the central non-conducting barrier region is calculated in the presence of screening to characterize the electrostatic-gate control of the resonant-energy levels. A nonequilibrium Green function calculation determines the gate-dependent nonlinear current and quantifies the transistor effect also in the presence of scattering. Finally, we identify conditions when conservation laws ensure important transistor robustness, i.e., insensitivity to scattering and room-temperature operation.

Keywords: Nanoelectronics, nanotube resonant-tunneling transistor, screening in molecules.

[1]Corresponding author, E-mail: `hyldgaar@fy.chalmers.se`

1. Introduction

"There is Plenty of Room at the Bottom" [1] and fullerene nanotubes [2, 3] are showing promise for future nanoelectronics applications. The nature of conduction — metallic versus semiconducting — can be controlled by the local chiral structure [4, 5] of the nanotube. Fullerene materials assembled between metal contacts thus offer important nanoelectronics devices ranging from the extended all-semiconducting nanotube transistors [6] based on semiclassical transport [7] to compact (all-nanoscale) single-electron transistors [8] and the current-rectifying diodes [9] that arise with well-defined metal-semiconductor nanotube junctions. Such junctions are produced when topological defects connect nanotube sections of different local chiral structure[10] at experimentally observable kinks [9]. The experimental observation of double-heterojunction nanotubes [9] and proposals for active nanotube heterostructure fabrication [11] opens the possibility for a new type of band-structure engineering that could produce both nanotube quantum-dots devices [12] and robust, *i.e.,* scattering- and temperature-insensitive, nanotube resonant-tunneling transistors [13].

Here we detail calculations of the nonlinear and interacting current [14, 15, 16, 17] that arise within the nanotube-heterostructure transistor [13]. This paper explains how, for a sufficiently small tunneling system, the fundamental conservation of charge itself ensures tolerance towards finite-(room-)temperature operation and towards the strong inelastic scattering that the nonequilibrium operating conditions produce [18].

2. The nanotube-heterostructure resonant-tunneling transistor

Figure 1 show a sample nanotube-heterostructure transistor realization and illustrate the operation as a gate-controlled current-switch/transistor device. In short, the transistor device is of a field-effect design [7] but replaces the semi-classical transport operation by a quantum-mechanical one — nonequilibrium resonant tunneling [19]. A *nanoscale* section $L_{\rm B} \approx 3$ nm of semiconducting-fullerene transport barrier (central honeycomb region) traps a (lowest unoccupied molecular) resonant level (orbital) $E_{\rm orb}$ between metallic-nanotube leads ('L' and 'R')

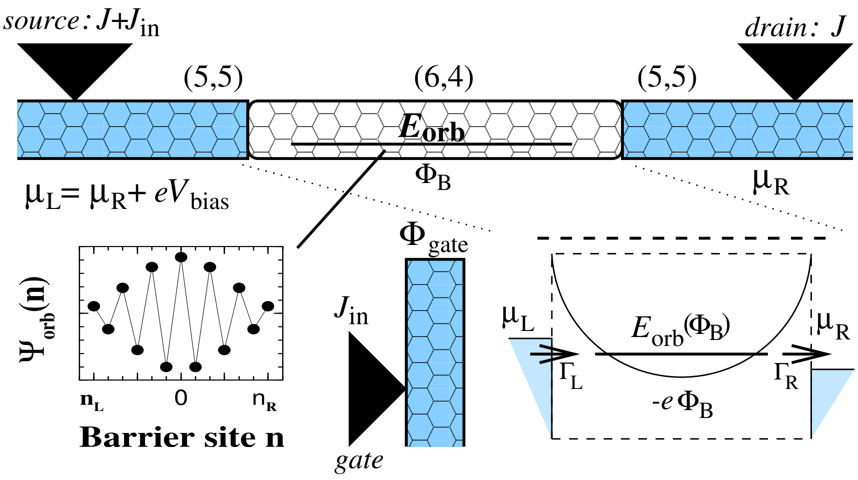

Figure 1: Sample realization of robust nanotube-heterostructure transistor. Nanotube dimensions and separations are shown to relative scale. A short, $L_B \approx 3$ nm, section of semiconducting-nanotube barrier (central honeycomb region) separates a pair of metallic-nanotube leads (horizontal grey tubes) kept at different chemical potentials $\mu_{\rm L/R}$ by source and drain contacts (upper triangles). The semiconducting barrier traps a lowest resonance orbital $\Psi_{\rm orb}$, *left insert,* with energy position $E_{\rm orb}$ controlled by a close metal gate (vertical grey tube) at voltage $\Phi_{\rm gate}$. *The right insert* illustrates the transistor-gate control. The semiconductor gap (dashed box) inhibits transport at $\Phi_{\rm gate} \sim 0$. However, a finite gate voltage, $\Phi_{\rm gate} \approx 2$ V, can suppress the electrostatic potential Φ_B inside the semiconducting barrier section, adjusts the resonant-level energy position $E_{\rm orb}$ (solid line), enable tunneling $\Gamma_{\rm L/R}$ (arrows), and produce a strong load current (drain-to-source) $J < J_{\rm RT} \sim 5\ \mu$A.

kept at different chemical potentials $\mu_{\rm L/R}$. A close gate at voltage $\Phi_{\rm gate}$, controls the resonance energy position $E_{\rm orb}$, and to a much smaller extend [13], the resonance-to-lead tunneling rates $\Gamma_{\rm L/R}$ ($\approx$ 10 meV at operating conditions). At $\Phi_{\rm gate} \sim 0$ the semiconducting-barrier gab $E_{\rm g} \approx 1$ eV (dashed box in panel) inhibits transport. However, a finite gate voltage $\Phi_{\rm gate}$ can suppresses the resonance-energy level to enable a strong resonant-tunneling (source-to-drain) load current

$$J \leq J_{\rm RT} \equiv \left(\frac{e}{\hbar}\right) \frac{4\Gamma_{\rm L}\Gamma_{\rm R}}{\Gamma_{\rm L}+\Gamma_{\rm R}} \sim 5\ \mu{\rm A}, \tag{1}$$

The (gate-to-source) input current is proportional to the resonant-level electron occupation [20]

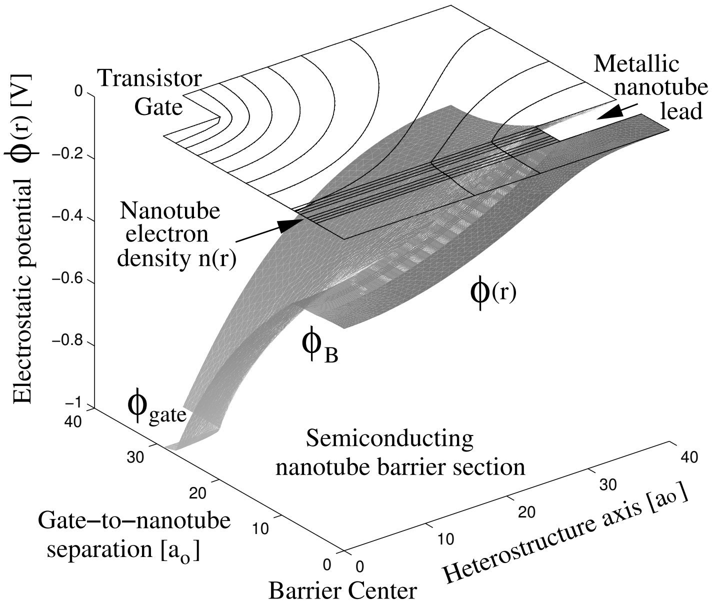

Figure 2: Electrostatic-field gate control of the nanotube-heterostructure transistor; Fig. 1. The figure specifies (sample) gate-to-nanotube separation in atomic units (a_0) and shows calculated spatial variation in the gate-induced electrostatic potential $\Phi(r)$ within a cut along the nanotube-heterostructure axis and out towards the external gate at $\Phi_{\rm gate}$; the potential is fixed at the metallic-nanotube leads. The finite density of electrons $n(r)$ (local variation indicated by parallel lines) inside the semiconducting barrier produces significant screening, Eq. (3). Nevertheless, we find that the external gate can suppress the barrier potential $\Phi_{\rm B}$ (here $\Phi_{\rm B} \approx \Phi_{\rm gate}/3$) sufficiently to enable the transistor current.

$0 < \langle n_{\rm orb} \rangle < 2$ but remains negligible

$$J_{\rm in} = J_{\rm V} \langle n_{\rm orb} \rangle / 2 \ll 1 \text{ nA}, \tag{2}$$

as it is restricted by barrier-to-gate vacuum tunneling [20, 21] $J_{\rm V} \ll e\Gamma_{\rm L/R}$.

The transition to a quantum-mechanical operating principle is necessary because we desire a transistor realization with a (maximum) feature size $L_{\rm f} \approx 3L_{\rm B} \approx 10$ nm much smaller than in the semiclassical nanotube field-effect transistors [6]. We propose and emphasize [13] the resonant-tunneling transport mechanism (Fig. 1) because conservation laws can then ensure transistor robustness (for all sufficiently small nanotube-heterostructure realizations).

2.1 Nanotube electrostatic-gate control

Figure 2 summarizes our estimate of electrostatic field-effect control for nanotube-heterostructure devices. For the central barrier section, the local electrodynamic response is given by [22, 23]

$$\varepsilon(n(r),\omega) = 1 - \frac{4\pi e^2 n(r)/m}{\omega^2 - \omega_0^0}, \tag{3}$$

where m_e denotes the electron mass and where we used a density-functional theory (DFT) calculation to determine the variation in the nanotube electron density $n(r)$. A separate DFT calculation of the overall static (molecular) polarizability was used to establish the value for the frequency cut off $\omega_0 \approx 10$ eV. Fig. 2 documents that this screening is significant and has important effects on the variation of the electrostatic potential between the external gate and the metallic-nanotube leads. In our sample realization (Fig. 1) we estimate a gate-induced potential-suppression $e\delta\Phi_{\rm B} \approx -e\Phi_{\rm gate}/3$ of the barrier potential and, hence, that the gate voltage $\Phi_{\rm gate} \approx 2$ V provides sufficient adjustment to enable (at $e\delta\Phi_{\rm B} \sim E_g/2$) the resonant-tunneling transistor current (Fig. 1, right panel).

3. Robust nonlinear transistor current

Figure 3 shows the current-switch effect, $J \equiv J(\Phi_{\rm gate})$ (top panel), the transistor effect, $J \propto J_{\rm in}$ (bottom panel), and a possible negative-differential amplification effect, $\delta J \propto -\delta J_{\rm in}$ (bottom panel) for the sample nanotube heterostructure device; Fig. 1. The figure assumes an implicit electrostatic gate control that adjust (insert panel) the resonant-level position, $\mu_{\rm L} - E_{\rm orb}(\Phi_{\rm gate})$. We calculate the transistor and negative-differential amplification effects, bottom panel, by adding a separate nonequilibrium Green function calculation [15, 16] of the resonant-level occupation $\langle n_{\rm orb}\rangle$ and hence, Eq. (2), of the corresponding input current $J_{\rm in}$ (again as a function of the implicit gate control). The current-switch and transistor effects are further described in Ref. [13].

The predicted negative-differential amplification effect, $\delta J \propto -\delta J_{\rm in}$ (bottom panel) could

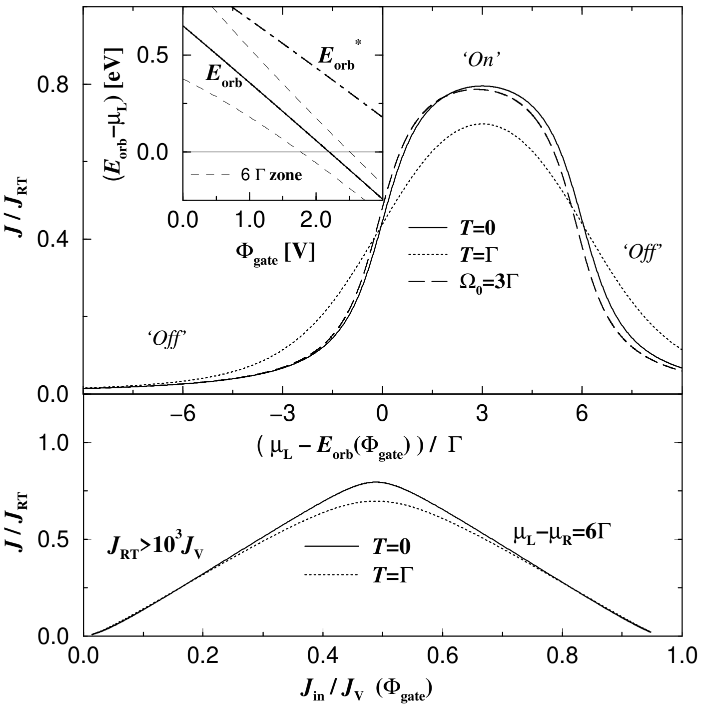

Figure 3: Robust transistor operation illustrated at a bias $eV_{\rm bias} = \mu_{\rm L} - \mu_{\rm R} = 6(\Gamma_{\rm L} + \Gamma_{\rm R})$. The *current-switch effect,* top panel, arises as the gate voltage $\Phi_{\rm gate}$ suppresses the lowest resonant-energy positions, $E_{\rm orb}$, $E^*_{\rm orb}\ldots$ (insert panel), increases the value of $\mu_{\rm L} - E_{\rm orb}(\Phi_{\rm gate})$, and enables J. A large ratio, $J_{\rm RT}/J_{\rm V} > 10^3$, describes the *transistor* and the *negative-differential amplification* effects, bottom panel. *Device robustness,* is emphasized (top panel) by contrasting the noninteracting estimate (4) (solid curve) against the current calculated at $T = \Gamma_{\rm L} + \Gamma_{\rm R}$ (dotted curve), and in the presence of a strong nonequilibrium scattering (dashed curve).

help realize ultrafast (THz) electron oscillators. This negative-differential amplification effect (bottom panel) arises when, at large gate voltages, the resonant-level occupation saturates, $\langle n_{\rm orb}\rangle \to 2$, while, at the same time, the resonant transport $J(\Phi_{\rm gate})$ (top panel) decrease with $\mu_{\rm L} - E_{\rm orb}$. We stress that the resonant-tunneling transport mechanism itself remains scattering insensitive [17] at oscillation frequencies $\hbar\omega_{\rm osc} \ll (\mu_{\rm L} - E_{\rm orb})$. The tunneling rates constitute a conservative limit, $\hbar\omega_{\rm osc} < \Gamma_{\rm L/R}$, for use of the negative-differential amplification effect.

All of these effects are quantified by combining our estimate of the electrostatic-gate control with an effective tight-binding Hamiltonian model within which we perform conserving nonequilibrium Green function calculations [14, 15, 16, 17]. For the sample heterostructure transistor realization (Fig. 1) we define and solve this effective tight-binding transport model as follows. The metallic-nanotube leads are described as 'armchair' structures [24] comprising rings of carbon atoms repeated every distance $\sqrt{3}d$ (d = 0.142 nm). The pair $\eta = 1, 2$ of metallic-nanotube transport channels is described [24] by associating each such ring with two tight-binding sites connected by effective overlap integrals $W_\eta = (-1)^\eta 2.66$ eV, respectively. For the (unoccupied) states in the central barrier region we use a similar description based on sites (here thirteen), enumerated along the wire, $n_{\rm L} \le n \le n_{\rm R}$, and connected by the overlap integral $t = 3|W_\eta|/4 - E_g/8 \approx 2$ eV. The corresponding barrier-site energies E_n are chosen to reflect the gate-induced electrostatic-field effects, $E_n(\Phi_{\rm gate})$ (here we take $n_{\rm R/L} = +/-6$ and $E_n(\Phi_{\rm gate}) \approx (-e\Phi_{\rm gate}/3) \times (n/7)^2$). For this tight-binding description of the isolated barrier we then use an exact diagonalization to estimate the gate control of the barrier resonances ($E_{\rm orb}, E_{\rm orb}*, \ldots$) and associated barrier-resonance wavefunctions ($\Psi_{\rm orb}(n), \ldots$). We obtain effective tunneling-escape rates [13] $\Gamma_{\rm L/R} \propto t|\Psi_{\rm orb}(n_{\rm L/R})|^2$ for which we can ignore the energy dependence.

3.1 Resonant-tunneling transistor transport

The insert panel of Fig. 3 shows, for the isolated barrier, the resulting estimates for the lowest/second-lowest energy levels (solid-dashed curves) as a function of the electrostatic gate control and documents that the nanoscale barrier $L_B \approx 3$ nm ensures a set of well-resolved transport resonances. The level separation $\delta E_{\rm orb}$ is inversely proportional to $L_{\rm B}$ and exceeds both the width of the resonance $\Gamma_{\rm L} + \Gamma_{\rm R}$ ($\approx$ 20 meV at operating condition for the sample transistor shown in Fig. 1) and the applied bias $eV_{\rm bias} = \mu_{\rm L} - \mu_{\rm R}$ (assumed at $6(\Gamma_{\rm L} + \Gamma_{\rm R})$. The transistor current is thus focused onto a single resonant level that support the robust nonlinear transport described below.

For the noninteracting case it is straightforward to estimate the resulting transistor transport [13, 15, 16, 17, 19, 25]. For a simple derivation we focus on the noninteracting single-resonance-level density of state (DOS), $N^0_{\rm orb}(E) = (\Gamma/\pi)/((E - E_{\rm orb})^2 + \Gamma^2)$ and emphasize that the difference in chemical potential produces a difference in occupation, $f_{\rm L/R}(E;T) = (\exp([\mu_{\rm L/R} - E)/T] + 1)^{-1}$ of left- and right-moving travelling state. At zero temperature, we obtain, a net noninteracting transistor-current estimate [19, 25]

$$J_0(E_{\rm orb}) = J_{\rm RT} \sum_{\rm X=L/R} S_X \arctan\left(\frac{\mu_{\rm X} - E_{\rm orb}}{\Gamma}\right), \tag{4}$$

where $S_{\rm L(R)} = +1/\pi\ (-1/\pi)$. The solid curve in the upper panel of Fig. 3 shows this zero-temperature noninteracting estimate for the transistor load current.

3.2 Device robustness by conservation laws

Figure 3 finally emphasizes that the nanotube-transistor is robust. This robustness implies that the predicted device characteristics are insensitive towards finite-temperature operation, defect scattering, and general nonequilibrium interactions. The top contrasts the load-current estimate (4) (solid curve) against a noninteracting current estimate evaluated at finite (room) temperature (dotted curve) and against a calculation of the interacting nonlinear device transport (dashed curve). For illustration we have here assumed a strong nonequilibrium coupling to a local phonon mode of energy $\Omega_0 = 60$ meV described by a electron-phonon interacting matrix element, $M_{\rm e-p} = 10$ meV. Neither temperature nor scattering cause changes in the transistor-load current, when

$$\delta E_{\rm B} \gg eV_{\rm bias} \equiv \mu_{\rm L} - \mu_{\rm R} \gg \max[T, \Gamma]. \tag{5}$$

This robustness results because conservation of charge ensures a simple sum rule for the interacting resonant-level DOS $N_{\rm orb}(E)$ *and* because this tunneling DOS can also define the interacting nonlinear transport. Since we can here ignore the energy dependence of the tunneling escape rates $\Gamma_{\rm L/R}$ we find (at general interacting conditions) a nonlinear resonant-tunneling current [15, 16, 17]:

$$J \approx J_{\rm RT} \int dE\ N_{\rm orb}(E)\,[f_{\rm L}(E;T) - f_{\rm R}(E;T)]. \tag{6}$$

There are important interacting-induces changes, $\delta N_{\rm orb}(E) = N_{\rm orb}(E) - N^0_{\rm orb}(E)$, in the DOS. However, these changes must, by a sum rule, integrate to zero. If, at sufficiently large applied biases, we can satisfy condition (5), the density-of-state sum rule will ensure a corresponding insensitivity of the predicted nonlinear transistor current (6).

The proposed nanotube-heterostructure transistors achieve device robustness, *i.e.,* an insensitivity towards scattering and finite-temperature operation, by their resonant-tunneling transport design. A nanoscale barrier extension L_{B} garanties a very large resonant-level separation $\delta E_{\mathrm{B}} \propto 1/L_{\mathrm{B}}$ and makes it straightforward to fullfill the robustness condition (5). All sufficiently small nanotube-heterostructure transistors can thus automatically achieve a robust operation.

4. Acknowledgements

We thank John W. Wilkins and Henrik Rydberg for highly valued comments and discussions. This work was supported by the Swedish Foundation for Strategic Research (SSF) through the Materials Consortium no. 9.

References:

[1] R. P. Feynman, *Engineering and Science* **Feb. 1960**, 22 (1960).

[2] S. Iijima, P. M. Ajayan, and T. Ichihashi, *Phys. Rev. Lett.* **69**, 3100 (1992).

[3] C. Dekker, *Phys Today* **May 1999**, 22 (1999).

[4] N. Hamada, S.-I. Sawada, and A. Oshiyama, *Phys. Rev. Lett.* **68**, 1579 (1992).

[5] C. T. White and J. W. Mintmire, *Nature* **394**, 29 (1998).

[6] S. J. Tans, A. R. M. Vershueren, and C. Dekker, *Nature* **393**, 49 (1998).

[7] C Weisbuch and B. Vinter, *Quantum Semiconductor Structures* (Academic Press, Boston, MA 1991), p. 142.

[8] H. Park *et al, Nature* **407**, 57 (2000).

[9] Y. Yao *et al*, *Nature* **402**, 273 (1999); supplement shows double-junction structure.

[10] R. Saito, G. Dresselhaus, and M. S. Dresselhaus, *Phys. Rev. B* **53**, 2044 (1996).

[11] D. Orlikowski *et al Phys. Rev. Lett.* **83**, 4132 (1999).

[12] L. Chico, M. P. L. Sancho, and M. C. Munoz, *Phys. Rev. Lett.* **81**, 1278 (1998).

[13] P. Hyldgaard and B. I. Lundqvist, *Solid State communications* **116**, 569 (2000).

[14] G. Baym, and L. P. Kadanoff, *Phys. Rev.* **124**, 287 (1961).

[15] S. Hershfield, J. H. Davies, and J. W. Wilkins, *Phys. Rev. Lett.* **67**, 3720 (1991).

[16] P. Hyldgaard *et al*, *Annals of Physics* **236**, 1 (1994).

[17] J. H. Davies *et al*, *Phys. Rev. B* **47**, 4603 (1993).

[18] P. Hyldgaard and J. W. Wilkins, *Phys. Rev. B* **53**, 6889 (1996).

[19] R. Tsu, and L. Esaki, *Appl. Phys. Lett.* **22**, 562 (1973).

[20] J. Bardeen, *Phys. Rev. Lett.* **6**, 57 (1961).

[21] E. Merzbacher, *Quantum Mechanics* (John Wiley & Sons, New York, 1970), pp. 124–133.

[22] A. Zangwill, *Physics at Surfaces* (Cambridge University Press, Cambridge, 1988), pp. 163–170.

[23] E. Hult *et al* *Phys. Rev. B* **59**, 4708 (1990).

[24] J. W. Mintmire, B. T. Dunlap, and C. T. White, *Phys. Rev. Lett.* **68**, 631 (1992).

[25] R. Landauer, *IBM J. Res.* **1**, 223 (1957).

FIGURE CAPTIONS

Figure 1: Sample realization of robust nanotube-heterostructure transistor. Nanotube dimensions and separations are shown to relative scale. A short, $L_B \approx 3$ nm, section of semiconducting-nanotube barrier (central honeycomb region) separates a pair of metallic-nanotube leads (horizontal grey tubes) kept at different chemical potentials $\mu_{\mathrm{L/R}}$ by source and drain contacts (upper triangles). The semiconducting barrier traps a lowest resonance orbital Ψ_{orb}, *left insert,* with energy position E_{orb} controlled by a close metal gate (vertical grey tube) at voltage Φ_{gate}. *The right insert* illustrates the transistor-gate control. The semiconductor gap (dashed box) inhibits transport at $\Phi_{\mathrm{gate}} \sim 0$. However, a finite gate voltage, $\Phi_{\mathrm{gate}} \approx 2$ V, can suppress the electrostatic potential Φ_B inside the semiconducting barrier section, adjusts the resonant-level energy position E_{orb} (solid line), enable tunneling $\Gamma_{\mathrm{L/R}}$ (arrows), and produce a strong load current (drain-to-source) $J < J_{\mathrm{RT}} \sim 5\ \mu$A.

Figure 2: Electrostatic-field gate control of the nanotube-heterostructure transistor; Fig. 1. The figure specifies (sample) gate-to-nanotube separation in atomic units (a_0) and shows calculated spatial variation in the gate-induced electrostatic potential $\Phi(r)$ within a cut along the nanotube-heterostructure axis and out towards the external gate at Φ_{gate}; the potential is fixed at the metallic-nanotube leads. The finite density of electrons $n(r)$ (local variation indicated by parallel lines) inside the semiconducting barrier produces significant screening, Eq. (3). Nevertheless, we find that the external gate can suppress the barrier potential Φ_{B} (here $\Phi_{\mathrm{B}} \approx \Phi_{\mathrm{gate}}/3$) sufficiently to enable the transistor current.

Figure 3: Robust transistor operation illustrated at a bias $eV_{\rm bias} = \mu_{\rm L} - \mu_{\rm R} = 6(\Gamma_{\rm L} + \Gamma_{\rm R})$. The *current-switch effect,* top panel, arises as the gate voltage $\Phi_{\rm gate}$ suppresses the lowest resonant-energy positions, $E_{\rm orb}, E^*_{\rm orb}\ldots$ (insert panel), increases the value of $\mu_{\rm L} - E_{\rm orb}(\Phi_{\rm gate})$, and enables J. A large ratio, $J_{\rm RT}/J_{\rm V} > 10^3$, describes the *transistor* and the *negative-differential amplification* effects, bottom panel. *Device robustness,* is emphasized (top panel) by contrasting the noninteracting estimate (4) (solid curve) against the current calculated at $T = \Gamma_{\rm L} + \Gamma_{\rm R}$ (dotted curve), and in the presence of a strong nonequilibrium scattering (dashed curve).

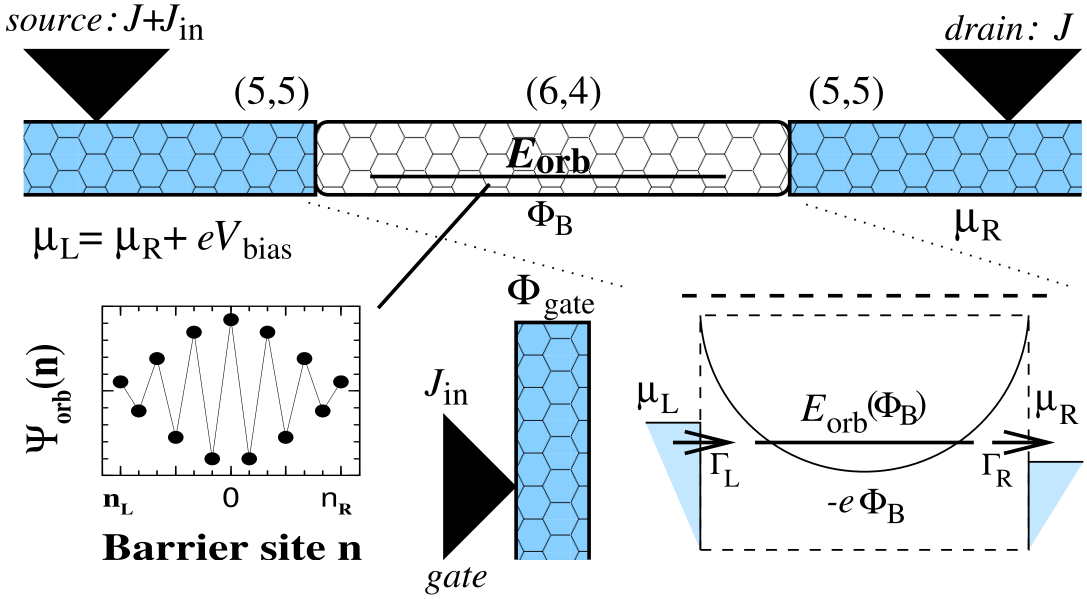

source : J+J_in
drain: J
(5,5)
(6,4)
(5,5)
E_orb
Φ_B
μ_L= μ_R+ eV_bias
μ_R
Ψ_orb(n)
n_L
0
n_R
Barrier site n
Φ_gate
J_in
gate
μ_L
μ_R
E_orb(Φ_B)
Γ_L
Γ_R
-eΦ_B

Figure 1

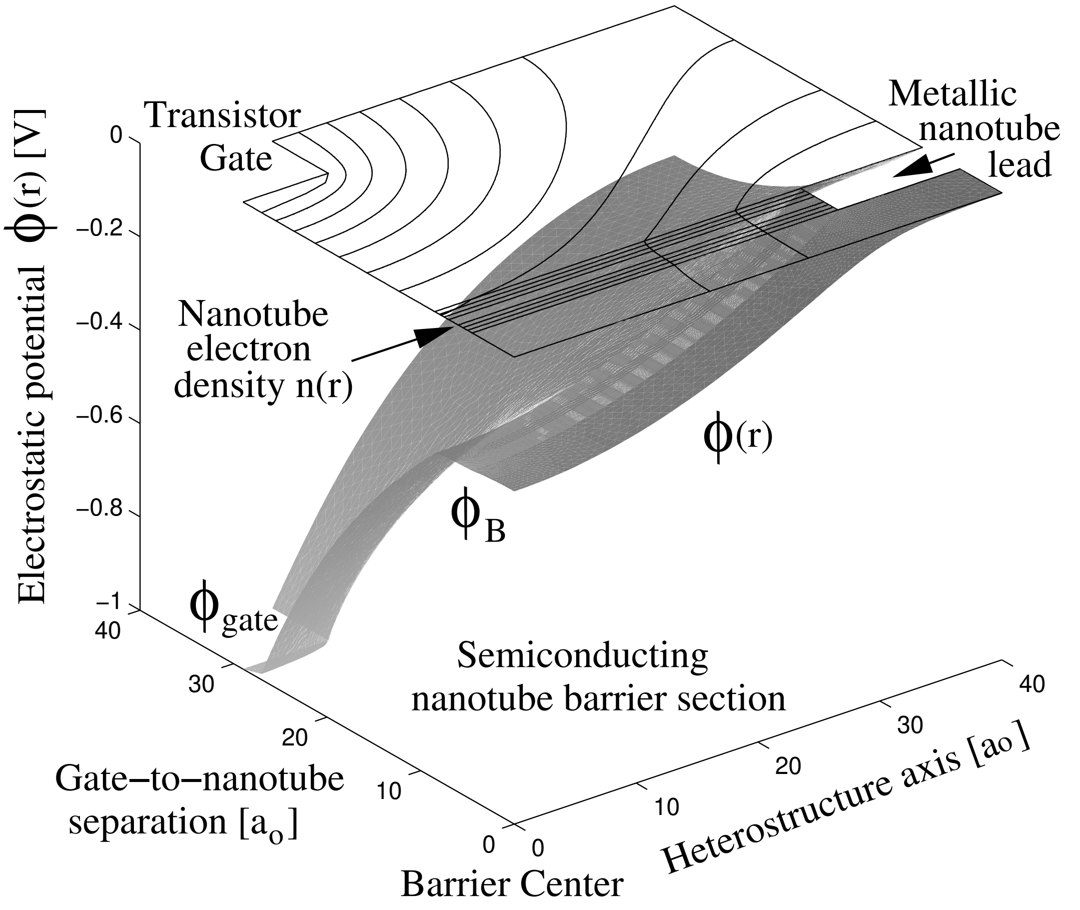
Transistor
Gate
Metallic
nanotube
lead
Nanotube
electron
density n(r)
ϕ(r)
ϕ_B
ϕ_{gate}
Electrostatic potential ϕ(r) [V]
0
−0.2
−0.4
−0.6
−0.8
−1
40
30
20
10
0
Semiconducting
nanotube barrier section
Gate−to−nanotube
separation [a_o]
Barrier Center
0
10
20
30
40
Heterostructure axis [a_o]

Figure 2

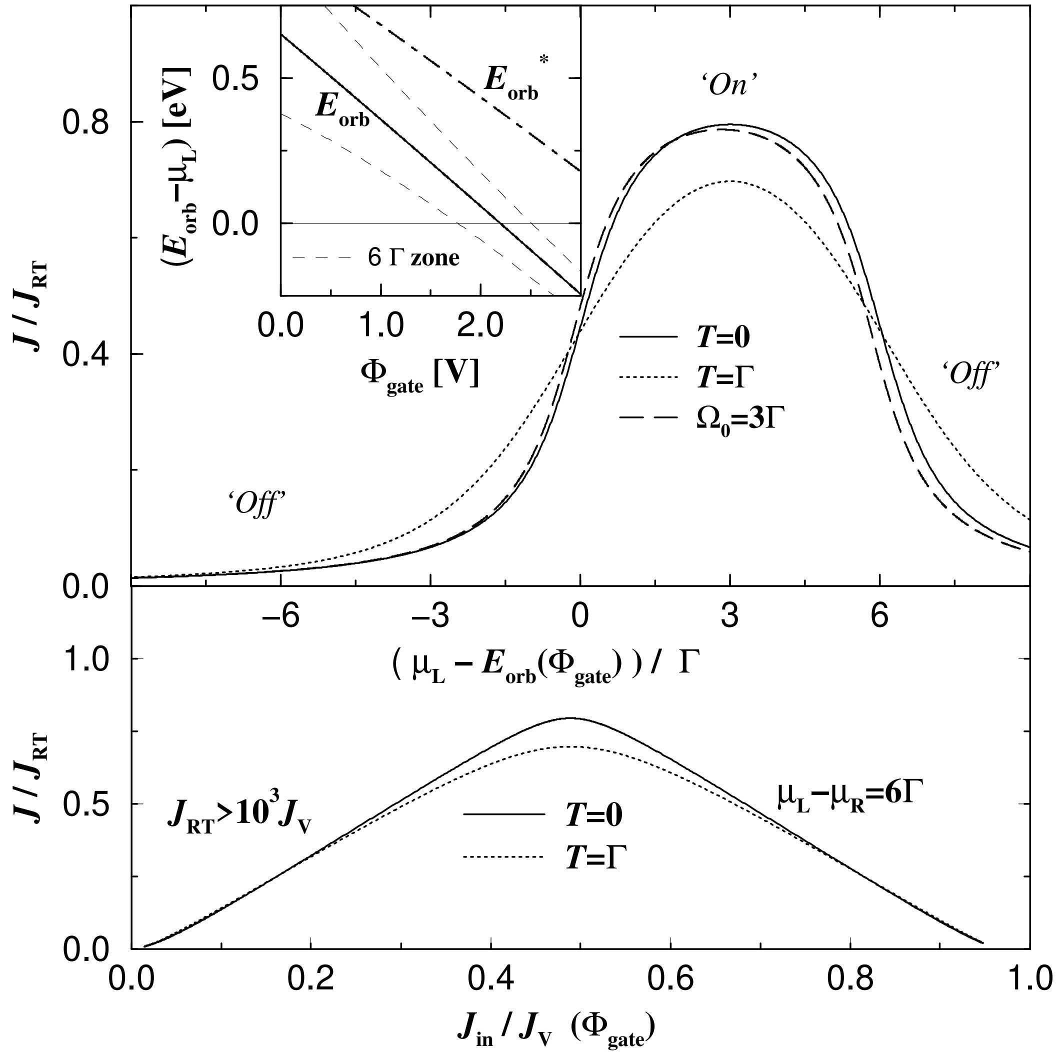

0.8
0.4
0.0
J / J_RT
'On'
'Off'
'Off'
T=0
T=Γ
Ω_0=3Γ
(E_orb−μ_L) [eV]
0.5
0.0
E_orb
E_orb*
6 Γ zone
0.0
1.0
2.0
Φ_gate [V]
−6
−3
0
3
6
(μ_L − E_orb(Φ_gate)) / Γ
1.0
0.5
0.0
J_RT>10^3 J_V
μ_L−μ_R=6Γ
0.2
0.4
0.6
0.8
1.0
J_in / J_V (Φ_gate)

Figure 3